The Astronomical Journal, 127:1431–1440, 2004 March

INTERGALACTIC H II REGIONS DISCOVERED IN SINGG

E. V. Ryan-Weber,[1,2] G. R. Meurer,[3] K. C. Freeman,[4] M. E. Putman,[5] R. L. Webster,[1] M. J. Drinkwater,[6] H. C. Ferguson,[7] D. Hanish,[3] T. M. Heckman,[3] R. C. Kennicutt, Jr.,[8] V. A. Kilborn,[9] P. M. Knezek,[10] B. S. Koribalski,[2] M. J. Meyer,[1] M. S. Oey,[11] R. C. Smith,[12] L. Staveley-Smith,[2] and M. A. Zwaan[1]

Received 2003 August 13; accepted 2003 November 19

ABSTRACT

A number of very small isolated H II regions have been discovered at projected distances up to 30 kpc from their nearest galaxy. These H II regions appear as tiny emission-line objects in narrowband images obtained by the NOAO Survey for Ionization in Neutral Gas Galaxies (SINGG). We present spectroscopic confirmation of four isolated H II regions in two systems; both systems have tidal H I features. The results are consistent with stars forming in interactive debris as a result of cloud-cloud collisions. The Hα luminosities of the isolated H II regions are equivalent to the ionizing flux of only a few O stars each. They are most likely ionized by stars formed in situ and represent atypical star formation in the low-density environment of the outer parts of galaxies. A small but finite intergalactic star formation rate will enrich and ionize the surrounding medium. In one system, NGC 1533, we calculate a star formation rate of $1.5 \times 10^{-3}\ M_{\odot}\ \mathrm{yr}^{-1}$, resulting in a metal enrichment of $\sim 1 \times 10^{-3}$ solar for the continuous formation of stars. Such systems may have been more common in the past and a similar enrichment level is measured for the "metallicity floor" in damped Lyα absorption systems.

Key words: galaxies: halos — galaxies: star clusters — H II regions — intergalactic medium — stars: formation

1. INTRODUCTION

H II regions signifying the presence of highly ionizing OB stars are usually found in the luminous inner regions of galaxies (see, e.g., Martin & Kennicutt 2001). H II regions are also located in the faint outer arms of spirals (e.g., Ferguson et al. 1998b), and as single or multiple star-forming knots in narrow emission line dwarfs (H II galaxies). In each case, new stars are formed in the vicinity of an existing stellar population. However, recent observations by Gerhard et al. (2002) have spectroscopically confirmed an isolated compact H II region on the extreme outskirts of a galaxy (NGC 4388) in the Virgo Cluster. Several luminous Hα-emitting knots have also been discovered in a compact group in the A1367 Cluster (Sakai et al. 2002). In these cases it appears that the H II regions are due to newly formed stars where no stars existed previously, albeit in a galaxy cluster environment.

As they evolve, OB stars increase the metal abundance in their local environment. Absorption-line studies show that the intergalactic medium (IGM) and galaxy halos, including our own, are enriched (e.g., Chen et al. 2001; Tripp et al. 2002; Collins et al. 2003). Isolated H II regions provide a potential source for this enrichment. In situ star formation in the IGM offers an alternative to galactic wind models to explain metal enrichment hundreds of kiloparsecs from the nearest galaxy.

Here we present a number of very small isolated H II regions that have been discovered by their Hα emission in the narrowband images obtained by the NOAO Survey for Ionization in Neutral Gas Galaxies (SINGG). SINGG is an Hα survey of an H I–selected sample of nearby galaxies. The survey is composed of nearly 500 galaxies from the H I Parkes All-Sky Survey (HIPASS; Barnes et al. 2001; Meyer et al. 2003); of these, about 300 have been observed in Hα. Since a gaseous reservoir is a prerequisite for star formation, SINGG measures a broad census of star formation in the local universe. The H II regions appear as tiny emission-line objects at projected distances up to 30 kpc from the apparent host galaxy. H II regions are defined as isolated if they are projected at least twice the $\mu_R = 25$ mag arcsec^{-2} isophotal radius from the apparent host galaxy. This is typically much farther than outer disk H II regions in spiral galaxies (Ferguson et al. 1998b). In fact, for the systems discussed in detail here it is not totally clear whether the isolated H II regions are even bound to the apparent host, and hence we refer to them as "intergalactic." Their high equivalent widths (EWs) suggest they are due to newly formed stars where no stars existed previously.

In § 2, spectra are presented for five isolated H II region candidates in three systems. These five candidates are referred to as the spectroscopically *detected* emission-line objects or H II region candidates. All sources but one have Hα detected at a recession velocity comparable to that of the nearest galaxy; two sources are also detected in [O III] as further confirmation. These four objects are referred to as the spectroscopically *confirmed* isolated H II regions. Optical spectra and H I distributions for all three systems are described in § 3. In § 4 models of the underlying stellar population, scenarios for star formation, enrichment of the IGM, implications of the intergalactic star formation rate, and the possibility that isolated

[1] School of Physics, University of Melbourne, VIC 3010, Australia.
[2] Australia Telescope National Facility, CSIRO, P.O. Box 76, Epping, NSW 1710, Australia.
[3] Department of Physics and Astronomy, Johns Hopkins University, 3400 North Charles Street, Baltimore, MD 21218.
[4] Research School of Astronomy and Astrophysics (RSAA), Mount Stromlo Observatory, Cotter Road, Weston, ACT 2611, Australia.
[5] Center for Astrophysics and Space Astronomy, 389 UCB, University of Colorado, Boulder, CO 80309.
[6] Department of Physics, University of Queensland, Brisbane, QLD 4072, Australia.
[7] Space Telescope Science Institute, 3700 San Martin Drive, Baltimore, MD 21218.
[8] Steward Observatory, University of Arizona, 933 North Cherry Avenue, Tucson, AZ 85721.
[9] Jodrell Bank Observatory, University of Manchester, Macclesfield, Cheshire SK11 9DL, UK.
[10] WIYN Observatory, 950 North Cherry Avenue, Tucson, AZ 85719.
[11] Lowell Observatory, 1400 West Mars Hill Road, Flagstaff, AZ 86001.
[12] Cerro Tololo Inter-American Observatory (CTIO), Casilla 603, La Serena, Chile.

H II regions are progenitors of tidal dwarf galaxies are discussed. $H_0 = 75$ km s^{-1} Mpc^{-1} is used throughout.

2. OBSERVATIONS

Continuum R-band and narrowband Hα images of local gas-rich galaxies were taken with the CTIO 1.5 m telescope as part of SINGG. At least three images were taken in each band, with small ($\lesssim 1'$) dithers between images. Each image was processed through overscan and bias subtraction, followed by division by a flat field derived from both dome and twilight sky flats. The images in each band were aligned and combined. The R or narrowband image with the better seeing was convolved to match the poorer seeing of the other image, and then the R image was scaled and subtracted from the narrowband image to produce a net Hα image. The final images have a pixel scale of $0\farcs43$ pixel^{-1} and subtend a field of view of nearly $15'$. The properties of the SINGG images are given in Table 1. The table includes the 5 σ point-source detection limit and the large-scale surface brightness limit for both R and Hα images. The latter was determined from the rms variation in the mean background level determined in boxes 35 pixels on a side after iteratively clipping pixels that deviated by more than 5 times the pixel-to-pixel rms from each box. The box-to-box variation of the mean is less than 1% of the sky level in all cases.

The candidate isolated H II regions were identified as unresolved high-EW sources outside the optical disk of each galaxy. Individual exposures were checked, and candidates with sharp edges (likely due to cosmic-ray residuals) or bright continua were rejected. Aperture photometry was performed on each of the isolated H II regions in the flux-calibrated SINGG images using IDLASTRO routines in IDL, yielding Hα and R fluxes. Since the H II regions have high EW, the R count rates were corrected for Hα line emission using the formula

$$C'_R = C_R - \frac{T_R(\lambda)}{T_{\rm NB}(\lambda)} C_{\rm H\alpha}, \qquad (1)$$

where C'_R is the corrected R count rate, C_R and $C_{\rm H\alpha}$ are the measured count rates in the R and net Hα images, and $T_R(\lambda)$ and $T_{\rm NB}(\lambda)$ are the throughputs of each filter evaluated at the wavelength λ of Hα. For the spectroscopically detected cases, λ was taken from the spectra; otherwise we assumed that SINGG was detecting net Hα emission redshifted by the H I heliocentric radial velocity. The results are given in Table 2. The spectroscopically detected isolated H II regions have Hα fluxes in the range $(6.9\text{–}11) \times 10^{-16}$ ergs s^{-1} cm^{-2}. Assuming the distance to each isolated H II region is the same as the host galaxy in each system, the Hα luminosities are $4\pi D^2 f_{\rm H\alpha} = 3.5 \times 10^{36}$ to 3.5×10^{38} ergs s^{-1}. In most cases the isolated H II regions are barely detected in continuum emission in the SINGG R images, with a typical 5 σ detection limit of around 1×10^{-18} ergs s^{-1} cm^{-2} Å^{-1} (see Tables 1 and 2). Isophotal radii at $\mu_R = 25$ mag arcsec^{-2} were measured for each galaxy using the ELLIPSE task in IRAF. The galaxy–H II region separations are given as a function of these radii in Table 3.

Spectra of 11 isolated H II region candidates were obtained with the Double Beam Spectrograph (DBS) on the RSAA 2.3 m telescope in 2002 September. Because of the very low continuum flux of the emission-line objects, it was necessary to use a nearby star to align the slit on each H II region candidate in the DBS autoguider. Three 2000 s exposures were taken of each object. The spectra were reduced using standard procedures in IRAF. The dispersion of the red spectra (6000–7000 Å) was 0.55 Å pixel^{-1}, corresponding to a resolution of 1.1 Å pixel^{-1} or 50 km s^{-1}. The dispersion of the blue spectra (3500–5400 Å) was 1.1 Å pixel^{-1}, corresponding to a resolution of 2.2 Å pixel^{-1} or 150 km s^{-1}. An additional two exposures of the candidate H II region near ESO 149-G003 were obtained in 2003 October using the same DBS setup. These additional exposures have been combined with the first spectra to produce the result in Figure 1.

Five of the 11 observed isolated H II region candidates were detected. The nondetected candidates mostly have $F_{\rm H\alpha} < 4 \times 10^{-16}$ ergs cm^{-2} s^{-1} (with the exception of the candidate H II region near NGC 1314) and have a range of continuum fluxes. In each case the DBS red spectrum fully covers the narrowband SINGG filter range. Since the spectra do not confirm the reality of these six isolated H II region candidates, they will not be discussed further. Four of the five detected isolated H II regions have confirmed emission lines within the narrowband filter's passband that are close to the expected position of Hα (6563 Å) at recession velocities close to that of their respective host galaxies (measured from HIPASS; see Table 3, second column). The recession velocity measured from each Hα line is given in Table 2. Some isolated H II regions were also detected in [O III] λ5007, confirming that the emission seen in the SINGG images is indeed Hα. The presence of both Hα and [O III] lines in these cases places the isolated H II regions at comparable recession velocities to the galaxy (or galaxies)

TABLE 1
PROPERTIES OF R AND Hα SINGG IMAGES WITH ISOLATED H II REGION CANDIDATES

Target	Exposure Time (s)		Seeing	Detection Limit		Surface Brightness Limit	
	R	Hα	(arcsec)	R (ergs s^{-1} cm^{-2} Å^{-1})	Hα (ergs s^{-1} cm^{-2})	R (ergs s^{-1} cm^{-2} Å^{-1} arcsec^{-2})	Hα (ergs s^{-1} cm^{-2} arcsec^{-2})
HCG 16.....	360	1800	1.7	1.08×10^{-18}	1.48×10^{-16}	1.33×10^{-19}	1.51×10^{-17}
ESO 154-G023	360	1800	1.2	9.20×10^{-19}	7.54×10^{-17}	5.57×10^{-19}	1.20×10^{-17}
NGC 1314.....	360	1800	1.5	9.46×10^{-19}	1.19×10^{-16}	1.05×10^{-19}	9.29×10^{-18}
NGC 1533.....	480	1800	1.4	9.08×10^{-19}	9.96×10^{-17}	4.99×10^{-19}	1.17×10^{-17}
IC 5052	360	1800	1.4	1.23×10^{-18}	1.11×10^{-16}	2.46×10^{-19}	1.82×10^{-17}
ESO 238-G005	360	1800	1.3	1.01×10^{-18}	1.04×10^{-16}	9.38×10^{-20}	1.20×10^{-17}
ESO 149-G003	360	1800	1.7	1.25×10^{-18}	1.37×10^{-16}	2.72×10^{-19}	1.33×10^{-17}

NOTE.—The detection limit is the 5 σ point-source detection limit. The final two columns give the large-scale surface brightness limit calculated as described in the text.

TABLE 2
PROPERTIES OF ISOLATED H II REGION CANDIDATES WITH DBS SPECTRA

Candidate H II Region	m_R (AB mag)	R Flux (ergs s^{-1} cm^{-2} Å^{-1})	Hα Flux (ergs s^{-1} cm^{-2})	EW (Å)	Hα Lum. (ergs s^{-1})	Lines Detected	Velocity (km s^{-1})
HCG 16 No. 1	>23.5	$<1.08 \times 10^{-18}$	$(1.0 \pm 0.05) \times 10^{-15}$	>1764	3.5×10^{38}	Hα, [O III]	3634 ± 50
ESO 154-G023 No. 1	21.3 ± 0.1	$(7.6 \pm 0.5) \times 10^{-18}$	$(3.8 \pm 0.5) \times 10^{-16}$	51	1.3×10^{36}	None	...
NGC 1314 No. 1	21.9 ± 0.1	$(4.6 \pm 0.4.) \times 10^{-18}$	$(1.6 \pm 0.05) \times 10^{-15}$	431	5.2×10^{38}	None	...
NGC 1533 No. 1	23.1 ± 0.3	$(1.5 \pm 0.4) \times 10^{-18}$	$(1.1 \pm 0.5) \times 10^{-15}$	1113	5.8×10^{37}	Hα, [O III]	846 ± 50
NGC 1533 No. 2	22.0 ± 0.1	$(4.1 \pm 0.4) \times 10^{-18}$	$(6.8 \pm 0.5) \times 10^{-16}$	177	3.6×10^{37}	Hα	831 ± 50
NGC 1533 No. 3	22.6 ± 0.2	$(2.3 \pm 0.4) \times 10^{-18}$	$(6.4 \pm 0.5) \times 10^{-16}$	331	3.4×10^{37}	Not obs.	...
NGC 1533 No. 4	22.5 ± 0.2	$(2.5 \pm 0.4) \times 10^{-18}$	$(5.8 \pm 0.5) \times 10^{-16}$	262	3.1×10^{37}	Not obs.	...
NGC 1533 No. 5	>23.6	$<9.08 \times 10^{-19}$	$(5.0 \pm 0.5) \times 10^{-16}$	>1658	2.6×10^{37}	Hα	901 ± 50
IC 5052 No. 1	22.6 ± 0.3	$(2.4 \pm 0.5) \times 10^{-18}$	$(3.2 \pm 0.4) \times 10^{-16}$	143	1.3×10^{36}	None	...
IC 5052 No. 2	20.72 ± 0.05	$(1.34 \pm 0.05) \times 10^{-17}$	$(4.0 \pm 0.4) \times 10^{-16}$	31	1.7×10^{36}	None	...
ESO 238-G005 No. 1	23.1 ± 0.3	$(1.5 \pm 0.5) \times 10^{-18}$	$(1.4 \pm 0.6) \times 10^{-16}$	102	1.3×10^{36}	None	...
ESO 238-G005 No. 2	>23.5	$<1.3 \times 10^{-19}$	$(2.0 \pm 0.6) \times 10^{-16}$	>1778	1.9×10^{36}	None	...
ESO 149-G003 No. 1	20.39 ± 0.03	$(1.8 \pm 0.05) \times 10^{-17}$	$(6.9 \pm 0.5) \times 10^{-16}$	39	3.5×10^{36}	Hα?	949 ± 50

NOTES.—Spectroscopically detected isolated H II regions have velocities listed in the final column. The fluxes and equivalent widths are measured from the SINGG images. In three cases, in which the continuum flux is below the detection limit, the upper limit EW is given. The H II region candidates 3 and 4 of NGC 1533 are included in this and the following table even though no spectra were taken.

in each field and rules out the possibility that they are background emission-line systems. Spectra for the five detected isolated H II regions are given in Figure 1. The Hα spectra (red arm) have been normalized by the continuum-subtracted Hα fluxes from the SINGG images. The Hα line fluxes have not been corrected for [N II] contamination. For the FWHM $\sim$35 Å filters used in this study, we expect the combined [N II] $\lambda\lambda$(6548+6583) contamination to be less than 10% if the line flux ratio [N II] λ6548/Hα = 0.35. The [O III] line lies in the blue arm, and the flux calibration of the spectra is uncertain. Details of the three systems, which include the five spectroscopically detected isolated H II regions, are discussed in the next section.

In addition to the Hα images and spectra, Australia Telescope Compact Array (ATCA) H I maps are available for two systems, NGC 1533 and ESO 149-G003. The ATCA data reduction is detailed in Ryan-Weber et al. (2003b). The two data sets have restored beams of $68'' \times 65''$ and $79'' \times 61''$, respectively. The velocity resolution is 3.3 km s^{-1} and the rms noise is 3.7 mJy beam^{-1} per channel, corresponding to a 3 σ column density limit (over a line width of 40 km s^{-1}) of 3.2×10^{19} cm^{-2}.

3. THREE SYSTEMS WITH DETECTED ISOLATED H II REGIONS

3.1. *NGC 1533*

Figure 2 shows a Digitized Sky Survey (DSS) image of NGC 1533 overlaid with ATCA H I contours. The enlargement has the same contours overlaid on the Hα image, with

TABLE 3
ISOLATED H II REGION CANDIDATES WITH DBS SPECTRA

Host Galaxy	Velocity (km s^{-1})	Distance (Mpc)	Region No.	Separation kpc	Separation R_{25}	H II Region Position (J2000) R.A.	H II Region Position (J2000) Decl.	$N_{\rm H\,I}$ (cm^{-2})
HCG 16	3917	53	1	19	2.0	02 09 28	−10 07 16	...
ESO 154-G023	574	5.3	1	6.0	3.5	02 56 31	−54 31 35	2.8×10^{19}
NGC 1314	3936	52	1	131	15.2	03 23 12	−04 15 16	...
NGC 1533	785	21	1	33	4.0	04 10 13	−56 11 37	2.4×10^{20}
			2	33	4.0	04 10 14	−56 11 35	2.4×10^{20}
			3	31	3.8	04 10 17	−56 10 46	9.8×10^{19}
			4	16	2.0	04 10 11	−56 07 28	3.2×10^{20}
			5	20	2.5	04 10 15	−56 06 15	1.5×10^{20}
IC 5052	584	5.9	1	8.0	1.4	20 52 59	−69 12 27	$<3.2 \times 10^{19}$
			2	10	1.7	20 52 53	−69 16 22	$<3.2 \times 10^{19}$
ESO 238-G005	706	8.9	1	3.9	30	22 22 33	−48 25 42	2.4×10^{20}
			2	11	84	22 22 42	−48 27 53	$<3.2 \times 10^{19}$
ESO 149-G003	576(628)[a]	6.5	1	3.4	5.2	23 51 51	−52 34 34	$<3.2 \times 10^{19}$

NOTES.—The velocity is the heliocentric velocity of the host galaxy measured by HIPASS. The distance given is to the host galaxy: HCG 16 uses the mean recession velocity from Ribeiro et al. 1998, NGC 1533 uses the distance from Tonry et al. 2001, and all other galaxies use the Local Group corrected velocity. The projected separation in kiloparsecs (to the optical center) is calculated using this distance. The projected separation is also calculated as a fraction of R_{25}, the major axis of the isophote at $\mu_R = 25$ mag arcsec^{-2}. The H I column densities are measured from ATCA maps, at the position of the H II region candidates, where available. Units of right ascension are hours, minutes, and seconds, and units of declination are degrees, arcminutes, and arcseconds.

[a] Velocity of the Hα line in the galaxy measured from the same long-slit spectrum as the isolated H II region is 628 ± 50 km s^{-1}.

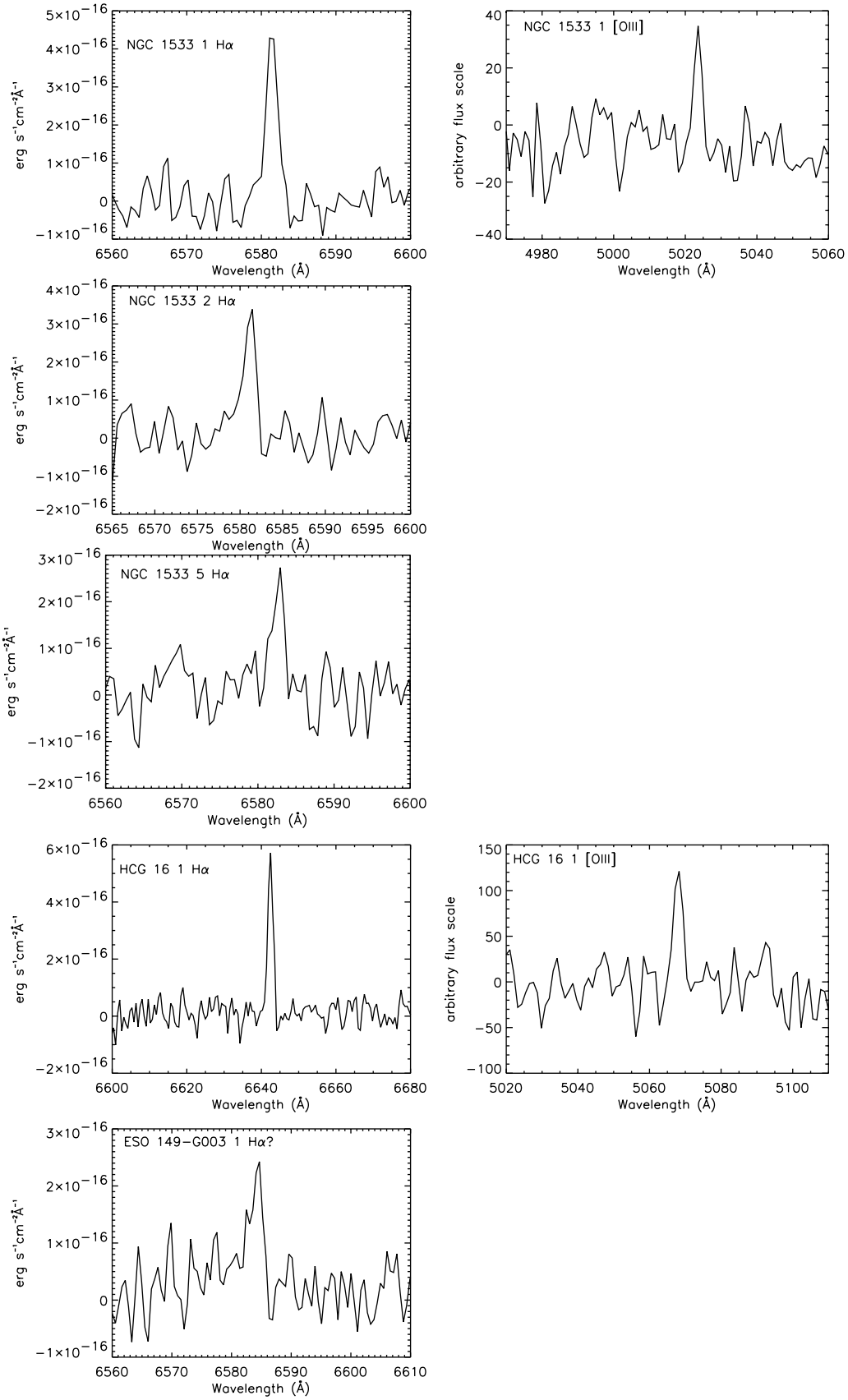

FIG. 1.—Emission lines from detected isolated H II region candidates: Hα (*left*) and [O III] (*right*). The Hα spectra have been normalized by the integrated Hα flux from the SINGG images given in Table 2; corrections for an [N II] component have not been made.

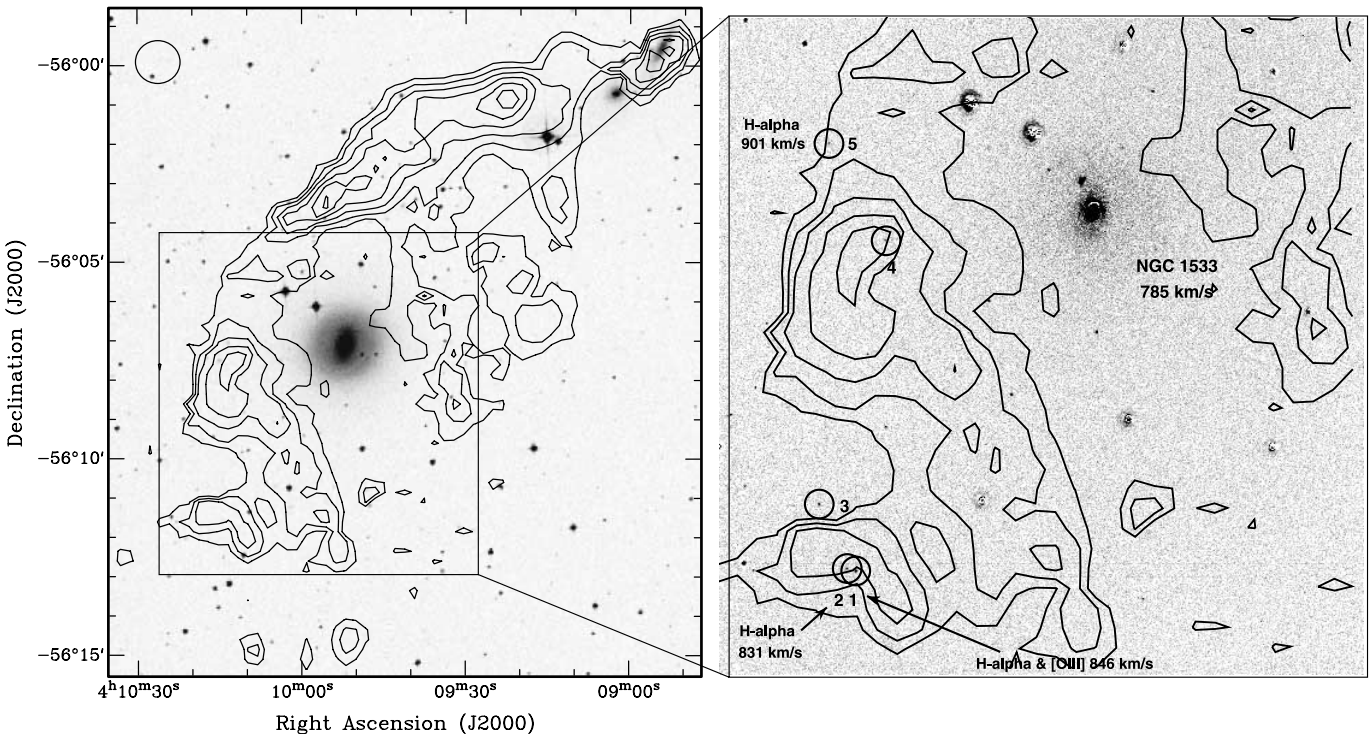

FIG. 2.—NGC 1533: DSS image with ATCA H I contours overlaid at 1.6, 2.0, 2.4, 2.8, 3.2, 3.6, and 4×10^{20} cm^{-2}. The beam is given in the upper left corner. The enlargement shows the continuum-subtracted Hα image with the isolated H II regions labeled and Hα velocities given, where available.

the isolated H II regions labeled. The H I distribution around NGC 1533 consists of two major arcs, the northwest cloud and the southeast cloud. H I gas with column densities below the lowest contour closes the H I in a ring. No obvious optical counterpart to this ring is seen in the DSS or in the *R* SINGG image. The total H I mass of the system (based on the total flux density from HIPASS of 67.6 Jy beam^{-1} km s^{-1}) is $7 \times 10^9\ M_\odot$. The southeast cloud contains about one-third of this total H I mass ($2.4 \times 10^9\ M_\odot$). The projected distance between the H I arcs and the optical center of NGC 1533 ranges from 2′ to 11.′7, corresponding to a projected physical length between 12 and 70 kpc.

NGC 1533 is an S0 galaxy located 1° from the center of the Dorado Group. The two smaller galaxies in the northwest corner of the image are IC 2039 (closest to NGC 1533, uncertain redshift, no H I detected) and IC 2038 (contains associated H I). The peculiar distribution of H I is thought to arise from the destruction of a galaxy to form a tidal remnant around NGC 1533. If the H I was stripped from IC 2038/2039, these galaxies would need to account for all the H I in the system and therefore have $M_{\rm H\,I}$-to-L_B ratios greater than 15, which is not very likely for their morphologies. The progenitor is more likely a low surface brightness (LSB) galaxy with a moderate H I mass, whose optical counterpart is now too diffuse to identify. *N*-body/SPH numerical simulations showing the orbital evolution of an LSB galaxy in NGC 1533's gravitational potential support this hypothesis (Ryan-Weber et al. 2003a).

The velocities of the three confirmed isolated H II regions (1, 2, and 5), 846, 831, and 901 km s^{-1}, compare well with the velocity of NGC 1533, at 785 km s^{-1}, and lie within the range of H I velocities in the southeast cloud (883 km s^{-1} with a width at 50% peak $w_{50} = 71$ km s^{-1}). Interestingly, the isolated H II regions do not appear to be correlated with the densest regions of H I and are located in the southeast cloud only. At this resolution (∼6 kpc), the densest region of H I is the central part of the northwest cloud. The stellar concentrations of tidal dwarf galaxies are located in the densest regions of H I, mapped in 21 cm at similar resolutions (∼4 kpc; see, e.g., Duc et al. 2000). Furthermore, the H I in the southeast cloud has velocity dispersions up to 30 km s^{-1} and velocity gradients in the range 7–50 km s^{-1} kpc^{-1}, making it an unlikely site for star formation. Star formation usually requires the gas to have a low velocity dispersion in order to collapse gravitationally.

3.2. *HCG 16*

The isolated H II region in the compact group HCG 16, shown in Figure 3, is near the two galaxies NGC 835 (SBab) and NGC 833 (Sa). The velocity of the isolated H II region (3634 km s^{-1}) sits on the lower edge of the H I emission measured by HIPASS (velocity 3917 km s^{-1}, $w_{50} = 288$ km s^{-1}, $w_{20} = 391$ km s^{-1}) and below the optical velocities of NGC 835 and NGC 833 (4073 and 3864 km s^{-1}, respectively, from the NASA/IPAC Extragalactic Database, NED). The two-dimensional spectrum shows the Hα emission line from NGC 833 at 3864 km s^{-1} and diffuse emission decreasing in velocity to ∼3700 km s^{-1} halfway along the line toward the isolated H II region. Verdes-Montenegro et al. (2001) have published a VLA map of HCG 16, showing H I in NGC 835 and NGC 833 with a large tidal feature to the northeast (overlapping the isolated H II region position) that joins other group members several arcminutes away to the east.

3.3. *ESO 149-G003*

The velocity of the isolated H II region candidate near the irregular galaxy ESO 149-G003 (949 km s^{-1}) is quite offset from its apparent host galaxy (H I velocity of 576 km s^{-1} and $w_{50} = 39$ km s^{-1}). The long-slit spectrum of the H II region

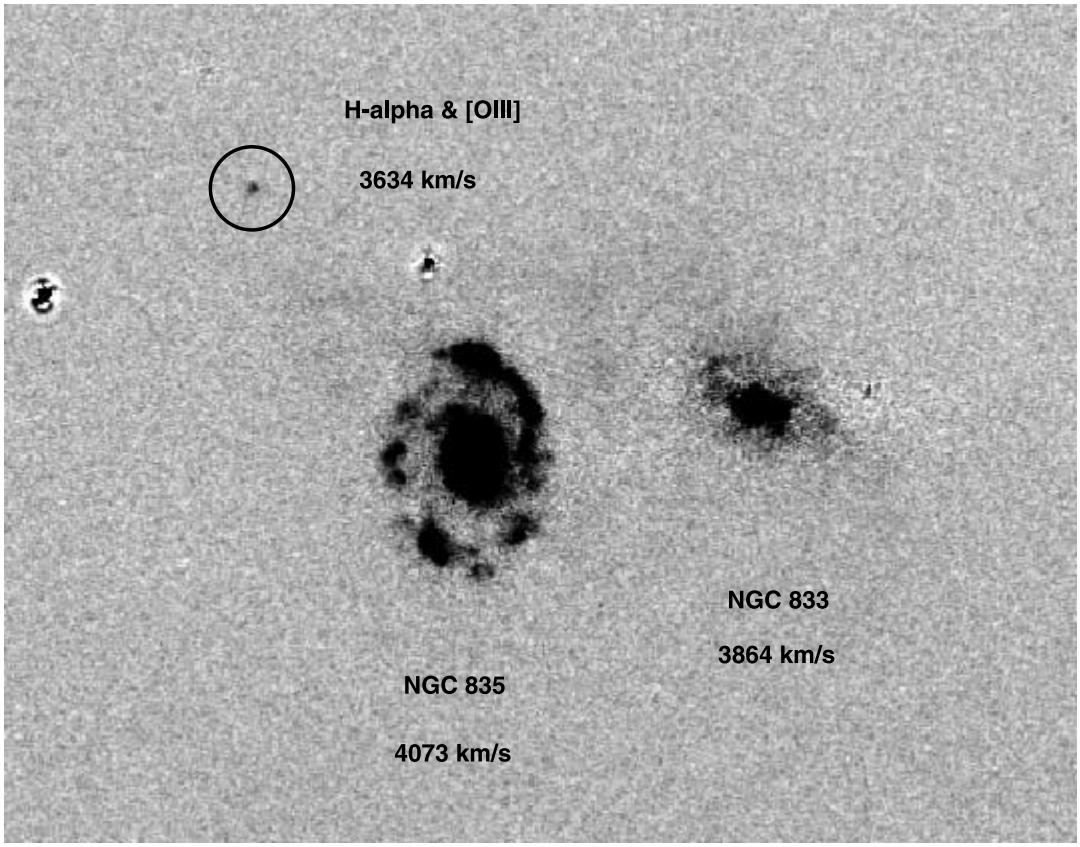

FIG. 3.—HCG 16: continuum-subtracted Hα image with the isolated H II region and two members of the galaxy group labeled. The two other objects in the field are residuals of foreground stars.

candidate also includes the southern part of the galaxy, and the galaxy's Hα emission line has a measured velocity of 628 $\pm$ 50 km s^{-1}. This 52 km s^{-1} deviation, just inside the quoted uncertainty, could be due to the slit's being aligned along the southern part of the galaxy only, although the H I spectrum does not show a large velocity gradient. A velocity difference of 321 km s^{-1} is measured between the galaxy and H II region candidate optical emission lines, assuming the single emission line is indeed Hα. The narrow H I profile shows no anomalous-velocity gas. Follow-up ATCA observations show no H I emission at the velocity and position of the emission-line object to $M_{\rm H\,I} \leq 8 \times 10^5$ (3×10^6) $M_\odot$ at a 3 σ limit, assuming a distance of 6.5 (12) Mpc. ESO 149-G003 seems quite isolated, and the nearest galaxy in both NED and HIPASS (Meyer et al. 2003) is ESO 149-G013 at 1500 km s^{-1}, 1.°6 ($\sim$560 kpc) away. However, ESO 149-G003 does show signs of a flared or warped optical disk at the edges, suggesting an interaction has taken place (see Fig. 4). A strong positive correlation between warping in late-type galaxies and environment (Reshetnikov & Combes 1998) has been largely attributed to tidal interactions. However, since only one emission line (Hα) is detected in this case, the possibility that this candidate isolated H II region is a background emission-line source cannot be ruled out, for example, Hβ at $z \sim 0.4$ or [O III] at $z \sim 0.3$.

4. DISCUSSION

4.1. *Underlying Stellar Population*

The Hα luminosities of the detected isolated H II regions (3.5×10^{36} to 3.5×10^{38}ergs s^{-1}) place them at the low-luminosity end of the H II region luminosity function (see, e.g., Oey & Clarke 1998). The Hα luminosity of an H II region is proportional to the ionizing photon luminosity (Q_0) above the Lyman limit (912 Å) from nearby stars. From equation (5.23) in Osterbrock (1989), $Q_0 = (\alpha_B/\alpha^{\rm eff}_{\rm H\alpha})(L_{\rm H\alpha}/E_{\rm H\alpha}) = 7.33 \times 10^{11} L_{\rm H\alpha}$, and using the ionizing luminosity of an O5 V star (Vacca et al. 1996), each isolated H II region is illuminated by the equivalent of 0.1–8 O5 V stars each. The least luminous detected isolated H II region can be ionized by a single O9.5 star.

The underlying stellar population is very weak in most of the spectroscopically detected emission-line objects; in two of the five cases it is undetected in the SINGG images. This makes it difficult to constrain whether the isolated H II regions are ionized by a single isolated massive star or whether the massive star or stars represent the "tip of the iceberg" of a cluster. A single massive star could have formed spontaneously; examples of this exist in the disk of the Milky Way where IR observations show an isolated massive star (Ballantyne et al. 2000). However, most massive stars form as part of a cluster (Clarke et al. 2000), with a characteristic initial mass function (IMF). The very low continuum emission does rule out a significant underlying stellar population and suggests that isolated H II regions are due to newly formed clusters where no stars existed previously. The low continuum emission also separates isolated H II regions from H II galaxies and tidal dwarf galaxies. Three of the four confirmed isolated H II regions have EW(Hα) $>$ 1000 Å. By comparison, H II regions in the outer arms of spiral galaxies (beyond the B 25th-magnitude isophote) measured by Ferguson et al. (1998a) have an average EW(Hα) of 364 Å. Furthermore, most of the group of

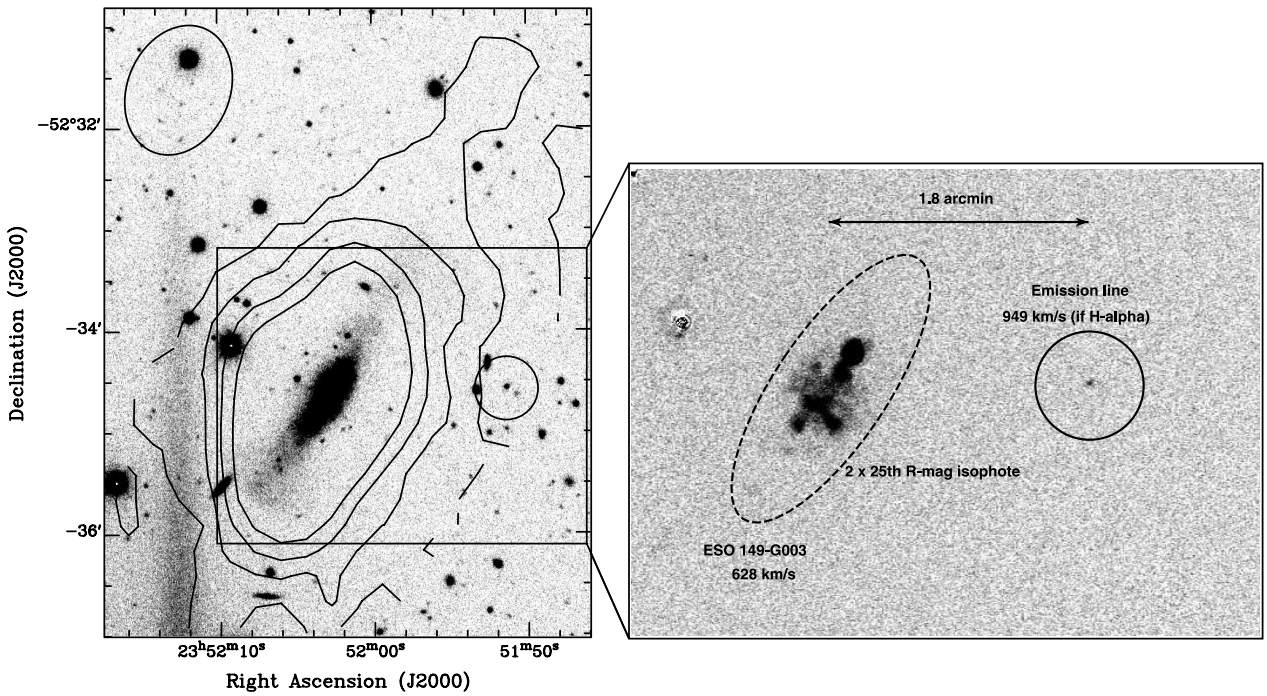

FIG. 4.—ESO 149-G003: *R* image with ATCA H I contours overlaid at 0.5, 1.0, 1.5, and 2.0 × 10^{20} cm^{-2}. The beam is given in the upper left corner. The enlargement shows the continuum-subtracted Hα image with the isolated H II region candidate and galaxy labeled.

star-forming dwarf galaxies in A1367 have EW(Hα) < 100 Å (Sakai et al. 2002).

Upper limit estimates of the underlying stellar population can be obtained from star formation models, such as Starburst99 (Leitherer et al. 1999). The ratio of Q_0 to the continuum luminosity, L_V, can be used to find the age of the population. Since very little continuum emission is detected from the isolated H II regions, the ratio Q_0/L_V is large, suggesting a very young age, in the range $(3-7) \times 10^6$ yr, for the parameters of the five detected H I regions. Indeed young ages are expected, since we selected isolated H II region candidates with high EW. Using the Starburst99 model with a Salpeter IMF, $M_{\rm up} = 100\ M_\odot$, and metallicity of 0.4 times solar, a very young instantaneous burst is predicted to have a photon luminosity in the range $\log Q_0(\text{photons s}^{-1}) = 51.3-2.7$ for a system with $10^6\ M_\odot$. The same model predicts (1.2–4.5) × 10^3 O stars (in the spectral range O3–O9.5). Scaling Q_0 with Q_0(H II region), the number of O stars ionizing each isolated H II region is in the range 4–7, corresponding to a total cluster mass of (0.9–1.8)×$10^3\ M_\odot$. The HCG 16 isolated H II region is significantly more luminous in Hα, and according to this model, it would consist of 23 O stars in a cluster of $5 \times 10^3\ M_\odot$. The ESO 149-G003 isolated H II region, unlike the others, does have considerable continuum emission in the *R* image (see Table 2). This suggests a slightly older population (7×10^6 yr) with 1.4 O stars and a cluster mass of $1.2 \times 10^3\ M_\odot$. These models account for the nebula emission in the continuum luminosity.

Continuous star formation models predict stellar population ages in the range $6 \times 10^6 - 1.5 \times 10^7$ yr for isolated H II regions with the largest equivalent widths (HCG 16 No. 1, NGC 1533 No. 1, and NGC 1533 No. 5). In these cases, the calculated ages are consistent with the instantaneous-burst models and confirm that the isolated H II regions are due to newly formed clusters where no stars existed previously. A stellar age of 3×10^8 yr is found for a continuous star formation model of NGC 1533 No. 2. The low EW of the candidate H II region in the ESO 149-G003 field however cannot be reasonably fitted by the continuous star formation models.

The calculations above assume a simple scaling of the number of ionizing stars with total cluster mass. At small cluster masses, the differences between analytic and stochastic IMFs can be substantial, especially in the number of high-mass stars. Statistical errors in stellar population models are discussed by Cerviño et al. (2002). Monte Carlo simulations can be used to investigate the effects of small initial masses on clusters. García Vargas & Díaz (1994) found the probability of finding a small cluster with an $M > 60\ M_\odot$ star is not zero, as suggested by the analytic IMF, but rises to 12%. Monte Carlo simulations by Cerviño & Mas-Hesse (1994) also obtain similar results. These simulations suggest that the total cluster mass calculated above could be overestimated.

4.2. *Origins of Isolated* H II *Regions*

Since we have just two systems with confirmed isolated H II regions, it is difficult to draw any conclusions on a common formation scenario, if one exists. Evidence of interactions, however, feature in all systems. NGC 1533 and HCG 16 both display tidally disrupted H I outside the main optical region of the galaxies. Although the isolated H II region projected to be near ESO 149-G003 could be a background object, if the two are associated the warping in ESO 149-G003's disk could indicate an interaction has occurred. The two systems that feature similar objects reported in the literature, NGC 4388 in the Virgo Cluster (Vollmer & Huchtmeier 2003; Gerhard et al. 2002) and A1367 (Sakai et al. 2002), also show disrupted H I. Vollmer & Huchtmeier (2003) use ram pressure stripping to explain the isolated H II region near NGC 4388. Ram pressure

stripping is less likely in our two systems, which occur in much less dense environments.

The projected separations between the isolated H II regions and host galaxies (see Table 3) suggest the underlying massive stars have mostly likely formed in situ. Alternatively, the stars could have formed in the galaxy and then been ejected. Typical ejection velocities due to dynamical interactions do not exceed 200–300 km s^{-1} (Leonard & Duncan 1988). However, the velocity required to travel 4–33 kpc in the lifetime of a massive star ($\sim 10^7$ yr) is 390–3200 km s^{-1}. The close match in velocity between the isolated H II regions and the galaxy, at least in the NGC 1533 system, suggests that the isolated H II regions are not currently moving at a high relative speed.

Our own Galactic halo has interactive H I debris that appears to be forming stars. The Magellanic Bridge is an H I complex that joins the Large and Small Magellanic Clouds at $\sim$50 kpc and represents the interaction between these two galaxies (e.g., Putman et al. 2003). Simulations indicate the Bridge was formed 200–500 Myr ago (e.g., Gardiner & Noguchi 1996), but the stars in the Bridge are between 10 and 25 Myr old (e.g., Demers & Battinelli 1998), indicating that star formation is currently active within this gas-dominated tidal feature.

We have three confirmed isolated H II regions with detailed H I information in the NGC 1533 system. The high-velocity dispersions and gradients in the vicinity of the isolated H II regions in this system suggest that star formation is not occurring via the usual gravitational-collapse mechanisms. Star formation could be shock-induced by clouds colliding (see, e.g., Zhang et al. 2001; Sato et al. 2000). Is it reasonable to expect collisions in the NGC 1533 system? Christodoulou et al. (1997) calculated the timescale for collisions in low-density environments such as Galactic high-velocity clouds and the Magellanic Stream and Bridge. Following Christodoulou et al. (1997), a cloud on a random walk with velocity dispersion σ_v has a characteristic time between collisions of $\tau_1 = l/\sigma_v$, where the mean free path $l = V/(N\pi R^2)$, that is, the volume (V) divided by the number of clouds (N) with cross section πR^2. Considering all clouds in the volume, the characteristic time between any two collision is $\tau_c = \tau_1/N = V/(N^2\pi R^2\sigma_v)$.

The H I ring around NGC 1533 appears to be clumped on scales of no greater than the resolution of the image ($\sim 1'$), corresponding to a radius of 3 kpc at a distance of 21 Mpc. Of course, the gas is likely to be clumped on smaller scales too, so this radius is an upper limit. The density, ρ, can be estimated from the surface density, $N_{\rm H\,I}$, where $\rho = m_{\rm H} N_{\rm H\,I}/(2R) = 1.8 \times 10^{-26}$ g cm^{-3}. The mass of each cloud is then given by $M_{\rm H\,I} = 4\pi\rho R^3/3 = 3.0 \times 10^7\ M_\odot$. Since the entire ring has an H I mass of $7 \times 10^9\ M_\odot$, it could be composed of 200 such clouds. The total ring surface area covered by H I with column densities greater than 2×10^{20} cm^{-2} is 4×10^3 kpc^2, assuming a thickness of at least a cloud diameter (6 kpc), which gives a volume estimate of 24×10^3 kpc^3. The velocity dispersion in the ring varies from 5 km s^{-1} in the northwest part to 30 km s^{-1} in the southeast. The timescale of a collision between any two clouds is, therefore,

$$\tau_c = 6.9 \times 10^5 \left(\frac{V}{24 \times 10^3\ \mathrm{kpc}^3}\right)\left(\frac{N}{200}\right)^{-2} \times \left(\frac{R}{3\ \mathrm{kpc}}\right)^{-2}\left(\frac{\sigma_v}{30\ \mathrm{km\ s^{-1}}}\right)^{-1} \mathrm{yr}. \quad (2)$$

This timescale varies between 1 and 4 Myr depending on σ_v (and is a lower limit for smaller cloud radii). The lifetime of an O star is only 1×10^7 yr, so we would expect to see two to 14 star formation events due to cloud collisions at any one time. This estimate agrees with the fact that we see five isolated H II regions in the NGC 1533 ring. This formation scenario is therefore plausible.

4.3. *IGM Enrichment*

Although the Hα luminosities are small, an estimate of the star formation rate can be obtained from the relation SFR($M_\odot$ yr^{-1}) = ($L_{\rm H\alpha}$/1.26 $\times$ 10^{41} ergs s^{-1}) (Kennicutt 1998). Summing the Hα luminosities from the five isolated H II regions in the NGC 1533 system, the SFR is $1.5 \times 10^{-3}\ M_\odot$ yr^{-1}. The other systems with only one isolated H II region are lower still. A small, but finite, intergalactic star formation rate will continually enrich and ionize the IGM. Maeder (1992) calculated the total yield (y) of metals expelled in winds and ejecta from supernovae and planetary nebulae. For a Salpeter IMF and a range of initial metallicities, they find $0.022 < y < 0.027$. Therefore, an SFR of $1.5 \times 10^{-3}\ M_\odot$ yr^{-1} will return $\sim 4 \times 10^{-5}\ M_\odot$ yr^{-1} of metals into the surrounding medium. Simulations of the dynamical evolution of H I gas around NGC 1533 show that it could last up to 1 Gyr (Ryan-Weber et al. 2003a). This is considered an upper limit, since no consumption of gas due to the formation of stars is taken into account. If the SFR is maintained for 1 Gyr, metals will pollute the $2.4 \times 10^9\ M_\odot$ of H I in the southeast cloud, resulting in a metallicity of $\sim 1 \times 10^{-3}$ times solar. Alternatively, if the SFR were not continuous and corresponded to a single population of stars only, the resulting metallicity would be negligible ($\sim 1 \times 10^{-6}$ times solar).

How does this compare to the abundances seen in Lyα absorption-line systems? H I in the vicinity of the NGC 1533 isolated H II regions has $N_{\rm H\,I} = 1$–4×10^{20} cm^{-2}, equivalent to a damped Lyα absorption (DLA; $N_{\rm H\,I} \geq 2 \times 10^{20}$ cm^{-2}) or sub-DLA system (10^{19} cm$^{-2} < N_{\rm H\,I} < 2 \times 10^{20}$ cm^{-2}). The metallicity of DLA or sub-DLA gas at low redshift varies from 0.01 times solar (e.g., I Zw 18; Aloisi et al. 2003) to solar. Depending on the initial metallicity, the isolated H II regions would enrich the NGC 1533 system by 10% at the most. At higher redshifts, however, this increase in metallicity could be more significant. Prochaska et al. (2003) find a DLA "metallicity floor" at $\sim 1.4 \times 10^{-3}$ times solar, over a redshift range from 0.5 to 5. Intergalactic star formation may have contributed to this. DLA systems with larger velocity widths are found to have higher metallicities (Nestor et al. 2003); this trend is also hinted at in the sub-DLA data (Peroux et al. 2004). Larger velocity widths may indicate interacting systems. In addition, since collisions and tidal disruptions of galaxies were more common at higher redshifts, the amount of high-$N_{\rm H\,I}$ gas outside galaxies was greater, and therefore the intergalactic star formation rate could have been higher in the past.

4.4. *Kinematics and the Tidal Dwarf Galaxy Connection*

Comparing the velocity of isolated H II regions with that of their apparent host galaxy and associated H I gas is useful in determining their dynamical connection. In Figure 5, the H I spectrum for each system is plotted with the velocity of the detected emission-line objects, assuming the line is indeed Hα. For the NGC 1533 system, the total H I profile in a beam area centered on the isolated H II region (or regions in the case

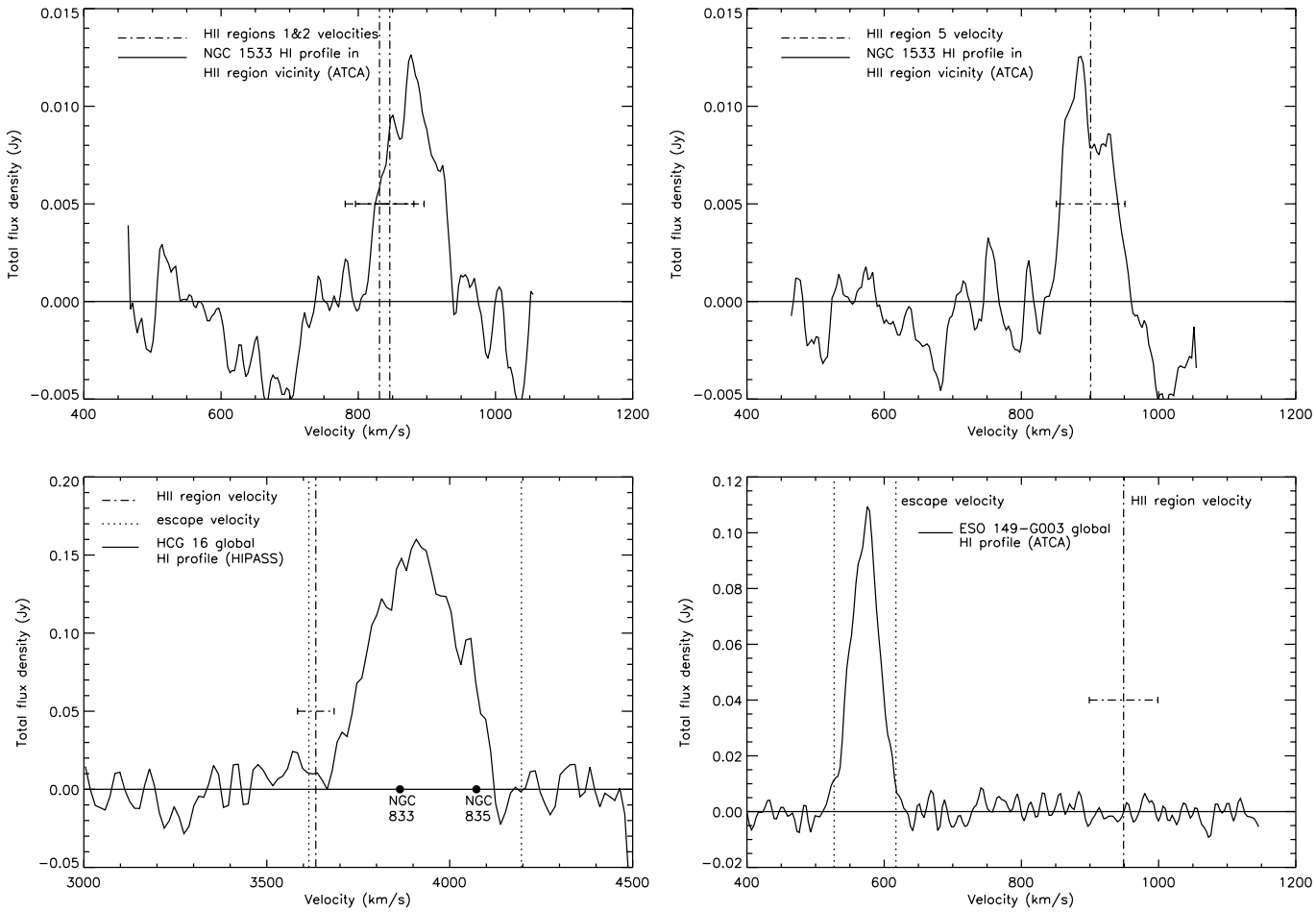

FIG. 5.—H I spectra of the three systems with detected isolated H II regions. The velocities of the H II region candidates are also plotted.

of 1 and 2, since they are so close) is given. The velocities of all three NGC 1533 confirmed isolated H II regions coincide well with H I gas, which is bound to and rotating around NGC 1533 (Ryan-Weber et al. 2003a). Are these isolated H II regions progenitors of tidal dwarf galaxies? Since the gas and isolated H II regions are bound to the galaxy, it is likely that the stars formed will also remain bound in the tidal debris. There is certainly a reservoir of gas from which more stars could form, so it is possible in this case that a tidal dwarf galaxy could emerge.

For the other two systems the global H I spectrum is given, since we do not have a synthesis map of HCG 16 and there is no H I detected at the position and velocity of the isolated H II region near ESO 149-G003. The galaxy escape velocity and velocity of the isolated H II region are plotted on each spectrum to determine their kinematic connection. The escape velocity is estimated by $v_{\rm esc} \sim 1/\sqrt{2} w_{20} \sin i$, where w_{20} is the width of the global H I profile at 20% of its height and i is the inclination of the galaxy. No inclination correction is made for HCG 16, since there is more than one galaxy embedded in the H I emission. In HCG 16 the velocity of the isolated H II region sits just inside the escape velocity of the system. It is unclear whether the stars formed will remain bound or whether they will disperse into the intragroup medium. The large difference in velocity between ESO 149-G003 and its candidate isolated H II region suggests the two are not bound. Of course, to form a tidal dwarf galaxy, tidal gas is needed; the nondetection of high column density H I gas in the vicinity of this H II region candidate rules out this possibility.

4.5. *ESO 149-G003: A True Isolated* H II *Region?*

The emission-line source near ESO 149-G003 could be a part of an associated extragalactic H I cloud (although technically H I clouds do not have optical counterparts). Its H I mass upper limit of $8 \times 10^5\ M_\odot$ has implications for the search for extragalactic H I clouds around other galaxies and in galaxy groups. For example, Zwaan (2001) searched analoges of the Local Group to a 4.5 σ limit of $7 \times 10^6\ M_\odot$ and found no significant extragalactic H I clouds. This may motivate the search for lower H I mass extragalactic clouds. This isolated H II region candidate is quite different from the others discussed in this paper. Only one emission line is detected (making the line identification ambiguous), the continuum flux is significantly higher, and the apparent velocity difference between ESO 149-G003 and the H II region candidate (assuming the detected emission line is in fact Hα; see Fig. 5) places it well outside the escape velocity of ESO 149-G003 (45 km s^{-1}). This kinematic evidence suggests that the source is perhaps a distant emission-line galaxy in the field, rather than being associated with ESO 149-G003. Whether the emission line is Hα at 995 km s^{-1} or another line at a higher redshift is uncertain. Indeed, we expect a contamination rate of background emission-line systems of roughly one per SINGG image, based on number statistics from Boroson et al. (1993), Cowie & Hu (1998), and Rhoads et al. (2000). If the

emission line is Hα, this object holds interesting implications for the census of intergalactic matter. Absorption lines along random lines of sight tell us that the IGM is generally clumped spatially and in velocity and shows a range of densities and metallicities. In future studies, isolated H II regions could be used as beacons for star-forming regions of the IGM. This would complement absorption studies along random sight lines and low spatial resolution H I emission observations of the IGM.

5. CONCLUSIONS

The discovery of intergalactic H II regions presented here and in other recent publications provides a small but finite source of enrichment and ionization of the IGM. In two cases, the fact that these emission-line objects are detected in both Hα and [O III] rules out the possibility that they are background emitters. The Hα luminosities imply that each isolated H II region is ionized by 4–7 O stars. If these stars have formed in situ, they represent atypical star formation in a low-density environment. The low level of continuum emission from three of four confirmed isolated H II regions suggests the stellar populations are very young and have formed where no stars existed previously. If part of a normal IMF, the corresponding total cluster mass would be $\sim 10^3\ M_\odot$. In two out of three systems, isolated H II regions are associated with tidal H I features, providing a reservoir of neutral gas. In one particular system, NGC 1533, the mass, distribution, and velocity dispersion of the H I suggest that the rate of star formation ($1.5 \times 10^{-3}\ M_\odot\ \mathrm{yr}^{-1}$) could be sustained by the collision of clouds. This would result an increase in the metal abundance by $\sim 1 \times 10^{-3}$ times solar. This is the same abundance level as seen in the DLA "metallicity floor" (Prochaska et al. 2003). The amount of intergalactic high column density H I and the rate of collision-triggered intergalactic star formation may have been higher in the past. Ongoing investigations into the metallicities and underlying stellar population of these and other isolated H II regions in the SINGG images will shed more light on their nature and origin.

This research has made use of the NASA/IPAC Extragalactic Database, which is operated by the Jet Propulsion Laboratory, California Institute of Technology, under contract with the National Aeronautics and Space Administration. The Digitized Sky Survey was produced at the Space Telescope Institute under US government grant NAGW-2166. The images of these surveys are based on photographic data obtained using the Oschin Schmidt telescope on Palomar Mountain and the UK Schmidt Telescope. The plates were processed into the present compressed form with the permission of these institutions. E. V. R-W. acknowledges support from an Australia Postgraduate Award. M. E. P. acknowledges support by NASA through Hubble Fellowship grant HF-01132.01 awarded by the Space Telescope Science Institute, which is operated by the Association of Universities for Research in Astronomy, Inc., under NASA contract NAS 5-26555. M. S. O. acknowledges support from National Science Foundation grant AST 02-04853. Helpful comments by the referee are gratefully acknowledged.

REFERENCES

Aloisi, A., Savaglio, S., Heckman, T. M., Hoopes, C. G., Leitherer, C., & Sembach, K. R. 2003, ApJ, 595, 760
Ballantyne, D. R., Kerton, C. R., & Martin, P. G. 2000, ApJ, 539, 283
Barnes, D. G., et al. 2001, MNRAS, 322, 486
Boroson, T. A., Salzer, J. J., & Trotter, A. 1993, ApJ, 412, 524
Cerviño, M., & Mas-Hesse, J. M. 1994, A&A, 284, 749
Cerviño, M., Valls-Gabaud, D., Luridiana, V., & Mas-Hesse, J. M. 2002, A&A, 381, 51
Chen, H., Lanzetta, K. M., Webb, J. K., & Barcons, X. 2001, ApJ, 559, 654
Christodoulou, D. M., Tohline, J. E., & Keenan, F. P. 1997, ApJ, 486, 810
Clarke, C. J., Bonnell, I. A., & Hillenbrand, L. A. 2000, in Protostars and Planets IV, V. Mannings, A. P. Boss, & S. S. Russell (Tucson: Univ. Arizona Press), 151
Collins, J. A., Shull, J. M., & Giroux, M. L. 2003, ApJ, 585, 336
Cowie, L. L., & Hu, E. M. 1998, AJ, 115, 1319
Demers, S., & Battinelli, P. 1998, AJ, 115, 154
Duc, P.-A., Brinks, E., Springel, V., Pichardo, B., Weilbacher, P., & Mirabel, I. F. 2000, AJ, 120, 1238
Ferguson, A. M. N., Gallagher, J. S., & Wyse, R. F. G. 1998a, AJ, 116, 673
Ferguson, A. M. N., Wyse, R. F. G., Gallagher, J. S., & Hunter, D. A. 1998b, ApJ, 506, L19
García Vargas, M. L., & Díaz, A. I. 1994, ApJS, 91, 553
Gardiner, L. T., & Noguchi, M. 1996, MNRAS, 278, 191
Gerhard, O., Arnaboldi, M., Freeman, K. C., & Okamura, S. 2002, ApJ, 580, L121
Kennicutt, R. C., Jr. 1998, ApJ, 498, 541
Leitherer, C., et al. 1999, ApJS, 123, 3
Leonard, P. J. T., & Duncan, M. J. 1988, AJ, 96, 222
Maeder, A. 1992, A&A, 264, 105
Martin, C. L., & Kennicutt, R. C., Jr. 2001, ApJ, 555, 301
Meyer, M., et al. 2003, MNRAS, submitted
Nestor, D. B., Rao, S. M., Turnshek, D. A., & Vanden Berk, D. V. 2003, ApJ, 595, L5
Oey, M. S., & Clarke, C. J. 1998, AJ, 115, 1543
Osterbrock, D. E. 1989, Astrophysics of Gaseous Nebulae and Active Galactic Nuclei (Mill Valley, CA: Univ. Science Books)
Peroux, C., Dessauges-Zavadsky, M., D'Odorico, S., Kim, T. S., & McMahon, R. G. 2004, MNRAS, 345, 480
Prochaska, J. X., Gawiser, E., Wolfe, A. M., Castro, S., & Djorgovski, S. G. 2003, ApJ, 595, L9
Putman, M. E., Staveley-Smith, L., Freeman, K. C., Gibson, B. K., & Barnes, D. G. 2003, ApJ, 586, 170
Reshetnikov, V., & Combes, F. 1998, A&A, 337, 9
Rhoads, J. E., Malhotra, S., Dey, A., Stern, D., Spinrad, H., & Jannuzi, B. T. 2000, ApJ, 545, L85
Ribeiro, A. L. B., de Carvalho, R. R., Capelato, H. V., & Zepf, S. E. 1998, ApJ, 497, 72
Ryan-Weber, E., Webster, R., & Bekki, K. 2003a, in The IGM/Galaxy Connection, ed. J. L. Rosenberg & M. E. Putman (Dordrecht: Kluwer), 223
Ryan-Weber, E. V., Webster, R. L., & Staveley-Smith, L. 2003b, MNRAS, 343, 1195
Sakai, S., Kennicutt, R. C., Jr., van der Hulst, J. M., & Moss, C. 2002, ApJ, 578, 842
Sato, F., Hasegawa, T., Whiteoak, J. B., & Miyawaki, R. 2000, ApJ, 535, 857
Tonry, J. L., Dressler, A., Blakeslee, J. P., Ajhar, E. A., Fletcher, A. B., Luppino, G. A., Metzger, M. R., & Moore, C. B. 2001, ApJ, 546, 681
Tripp, T. M., et al. 2002, ApJ, 575, 697
Vacca, W. D., Garmany, C. D., & Shull, J. M. 1996, ApJ, 460, 914
Verdes-Montenegro, L., Yun, M. S., Williams, B. A., Huchtmeier, W. K., del Olmo, A., & Perea, J. 2001, A&A, 377, 812
Vollmer, B., & Huchtmeier, W. 2003, A&A, 406, 427
Zhang, Q., Fall, S. M., & Whitmore, B. C. 2001, ApJ, 561, 727
Zwaan, M. A. 2001, MNRAS, 325, 1142